CONTROL OF LAMINAR AND TURBULENT SHEAR FLOWS USING PLASMA ACTUATORS

Jamey D. Jacob and Karthik Ramakumar
Mechanical Engineering Dept., University of Kentucky
Lexington, KY 40506-0503
jdjacob@uky.edu, krama0@engr.uky.edu

Rich Anthony and Richard B. Rivir
AFRL/PRTT
WPAFB, Dayton OH 45433
richard.anthony@wpafb.af.mil, richard.rivir@wpafb.af.mil

ABSTRACT

The use of AC discharge plasma actuators in flow control applications is experimentally investigated using PIV. Experimental observations include actuators in quiescent flow, a flat plate boundary layer, and a low pressure turbine blade cascade. The actuators are shown to generate a high velocity region near the wall downstream of the interface with large fluctuating components. Even in cases where the velocity increase is small due to a fast free-stream flow, the actuator still produces velocity fluctuations of significant size. The displacement and momentum thicknesses decrease in the downstream region of the actuator, however. In the turbine cascade, separation is completely eliminated and cross-stream vortical structures are observed.

INTRODUCTION

Plasma actuators, also known as discharge plasma, dielectric barrier discharge, and glow discharge actuators, offer unique options in shear flow control applications. A number of researchers have investigated plasma actuators over recent years, and the present work discusses further experimental investigations, both from a perspective of better understanding the underlying physical mechanisms of the actuator interaction with the flow and the development of a practical plasma flow control (PFC) device. Both River *et al.* (2003) and Suchomel *et al.* (2003) provide detailed reviews of the historical developments in PFC and can be referred to for further information. Some of the more recent developments in the state-of-the-art are presented here for reference, but a more detailed background can be found elsewhere (Jacob, 2004).

Recent results include McLaughlin *et al.* (2004) where plasma actuators were used to control the structure of the Karman vortex street by using feedback results from measurements of the shedding frequency to drive the actuator frequency. Corke *et al.* (2004) demonstrated the use of plasma actuators as virtual flaps and slats for airfoil flow control. Actuators located at the leading edge can control separation while actuators placed at the trailing edge can control lift. Post and Corke (2004) showed that plasma actuators can be used to control airfoil stall in a dynamic pitching motion. While drag was not measured, there was measurable improvement in the lift over the oscillation cycle using different modes of plasma actuation.

Enloe *et al.* (2004a, 2004b) presented numerous findings on the behavior of plasma actuators. Based on large scale integral measurements of thrust output, voltage and plasma emission measurements, and simulations, the authors make several interesting conclusions, including that the power input, P, to the plasma is nonlinear with the voltage drop, ΔV, across the dielectric, and that both the maximum induced velocity, u_{max}, and thrust, T, are proportional to input power, such that

$$T \propto u_{max} \propto P \propto \Delta V^{7/2} \tag{1}$$

In addition, their measurements found that the plasma has complex spatial and temporal structure, the creation of plasma occurs on both the positive and negative slopes of ΔV and is dependent upon $d\Delta V/dt$. Also, thrust is greater for a "positive" waveform as opposed to a "negative" waveform, even though the bulk plasma structure is the same. This observation implies that bulk heating is not the mechanism for thrust generation, as some researchers have previously speculated (the "positive" waveform appears to produce a more uniform discharge) (e.g., Leonov *et al.* , 2001). Their final conclusion is that the plasma induces an electrostatic body force on the surrounding fluid that is proportional to the net charge density and the strength of the electric field, as

$$\mathbf{F} = -(\epsilon_o/\lambda_D^2)\phi\mathbf{E} \tag{2}$$

such that the net charge charge density can be expressed as a function of the electric potential, where ϵ_o is the permittivity of free space and λ_D is the Debye length, respectively.

The purpose of the present work is to investigate the detailed structure of the induced flow generated by the PFC actuator, particularly turbulent characteristics, and demonstrate how this can be leveraged in the control of laminar and turbulent shear flow fields.

EXPERIMENTAL ARRANGEMENTS AND OBSERVATIONS

Plasma Actuator and Power Supply

The plasma actuators tested consisted of conductive copper strips separated by a 50 micron thick Kapton dielectric; typically widths were 1 cm with corresponding lengths of 10-20

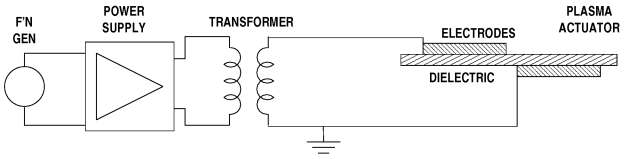

Figure 1: Plasma actuator schematic.

cm. A function generator is used to provide a sinusoidal input to either a bank of dual Titan Series power supplies with EIM-01 external input modules or a Kepco BPM-01 100 V power supply. The output drives an inductively matched step-up transformer (Industrial Test Equipment Company), capable of 6 kV output with 1-250 V RMS input at 1-7 kHz. The input power was monitored using a Tektronix TDS 3054B four channel oscilloscope while two Tektronix P6015A high voltage probes two Pearson Model 4100 current monitors were used for voltage and current measurements, respectively. The power supply/actuator schematic is shown in Figure 1. Note that the lower conductor is grounded; in the TRPIV boundary layer measurements conducted at AFRL, this conductor is instead driven with a voltage 180° out of phase with the upper conductor, thus resulting in a larger ΔV.

For the velocity field measurements, multiple PIV systems were used and detailed specifications are available elsewhere (Jacob *et al.*, 2004). One system recorded image pairs at a typical rate of 15 Hz while the other recorded at 300 Hz, allowing time-resolved measurements. These will simply be referred to as PIV and TRPIV (time-resolved PIV), respectively. In the PIV measurements presented herein, 62 realizations were used to develop statistics and mean flows for each run, while for the TRPIV measurements, 550 realizations were used.

The PIV algorithm used herein utilizes the wall adaptive Lagrangian parcel-tracking algorithm (WaLPT) developed by Sholl and Savaş (1997). This algorithm tracks the seeding as fluid parcels and determines their translations and deformations. Fluid parcels registered by CCD pixels are advected with individually estimated velocities and total accelerations. A standard DPIV algorithm is employed to determine the initial velocity field and the novel routines in WaLPT allow for more accurate measurement of the velocities near the wall by essentially mirroring the flow about the interface using an image parity exchange (IPX) routine (Tsuei and Savaş, 2000). Velocity and vorticity are calculated as part of the PIV algorithm and are scaled accordingly; vorticity is determined spectrally and does not suffer from typical numerical differentiation problems. One benefit of the WaLPT code is the ability to mask out surfaces within the flow field and apply the above mentioned IPX routine. In practice, this results in much higher accuracy of the wall derivatives which are particularly important when calculating boundary layer profiles and derived quantities such as skin friction coefficient.

Actuator in Quiescent Flow

Figure 2 shows the flow field developed by a PFC actuator in a quiescent flow. For this case, the plasma region was generated using a square wave with a frequency of 4.5 kHz and an amplitude of approximately 5 kV. Velocity fields were obtained using PIV and the FOV is approximately 5 cm square. One can easily see that the flow is being drawn into the plasma region by the plasma induced body force (equation 2). This results in a jet issuing to the right of the actuator. This is

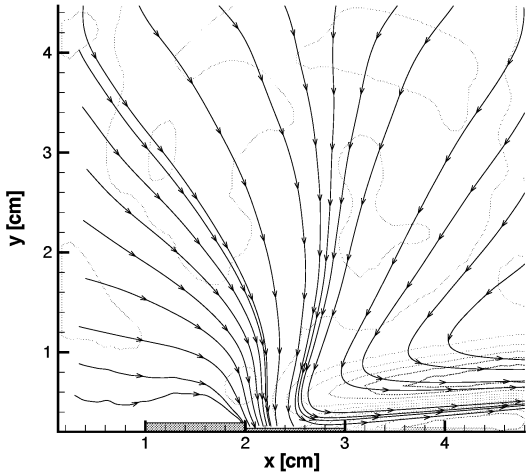

Figure 2: Plasma actuator in quiescent flow; streamlines. The actuator interface is located at the 2 cm tick.

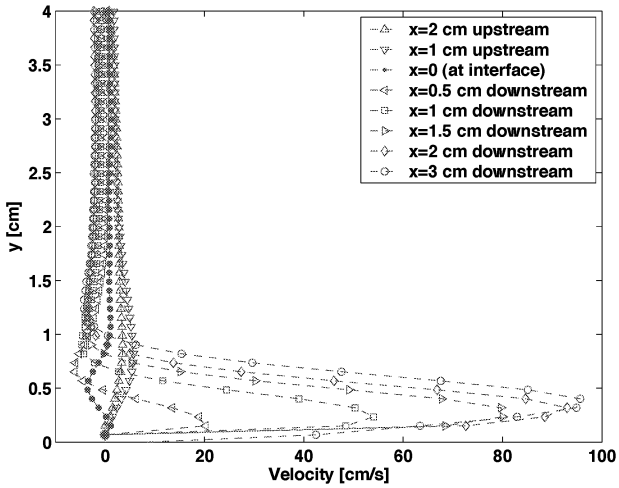

Figure 3: Plasma actuator in quiescent flow; velocity profiles.

seen more clearly in Figure 3 where profiles of the horizontal velocity u are plotted for 8 stations, including the actuator interface near the region of densest plasma. It is observed that at the interface, the velocity is still relatively small, and the magnitude at this point is largely due to the vertical downward component. As we proceed to the right of the actuator, the velocity increases as we travel "downstream" until we reach a maximum of 100 cm/s located 3 cm away from the interface. The width (or in this case, height) of the jet is confined to less than 1 cm away from the wall. The momentum within this jet is non-negligible, however.

The growth of the jet is linear with downstream distance from the interface from 0 to 2 cm and plateaus thereafter, as shown in Figure 4. If we examine the velocity fluctuations, shown in Figure 5 and normalized by the peak velocity, we see that large fluctuations are present within the jet, reaching nearly 35% 4 mm away from the wall. The large fluctuating component will be discussed in more detail below.

The actuators can be readily arranged such that compli-

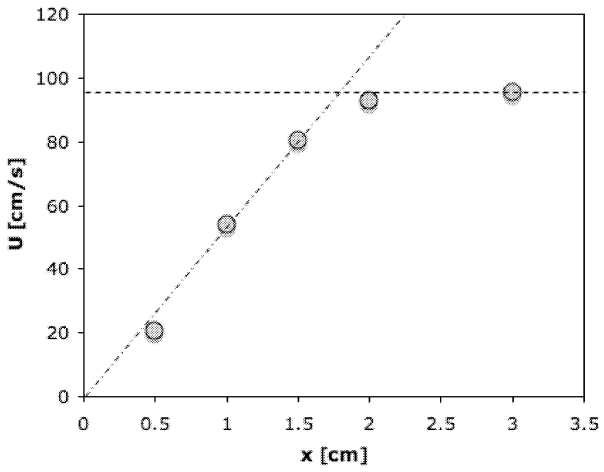

Figure 4: Growth of maximum velocity for actuator in quiescent flow.

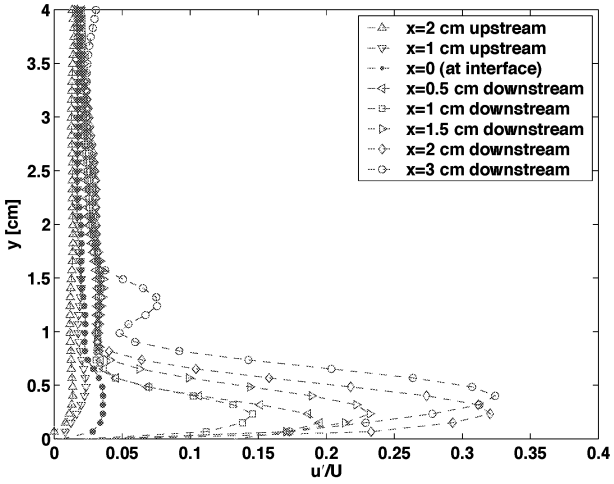

Figure 5: Plasma actuator in quiescent flow; velocity fluctuation profiles.

cated flow structures are created. Figure 6 shows the creation of a plasma induced synthetic jet by using an annular PFC actuator. These can be pulsed to create vortex rings or run continuously to create a steady synthetic jet.

Flat Plate Boundary Layer Modification

As shown in the previous section, a PFC actuator is capable of producing velocities up to at least 1 m/s very near the wall. Thus, we wish to examine the capability of the actuator in a flow field with free-stream velocities bracketing this velocity to determine how the plasma induced jet evolution varies with increasing free-stream velocity. To remove any other effects, the experiments were conducted using an actuator mounted onto a flat plate. Parameters are given in Table 1.

The low-speed boundary layer wind tunnel in PRTT at AFRL was used for the current experiments utilizing the TR-PIV system. The tunnel test section is constructed of acrylic and has a cross-section of 15×9.5 inches. Flow is generated by two fans in series and the inlet velocity is cooled by a heat

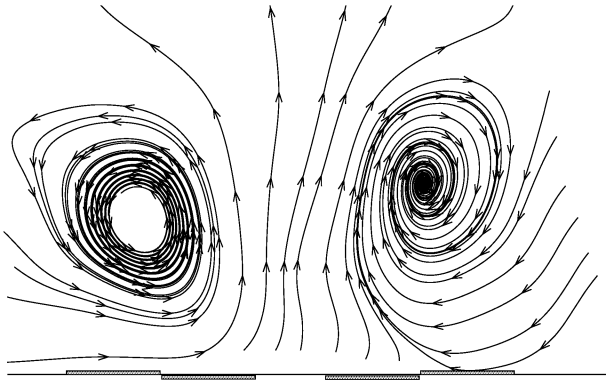

Figure 6: Vortex created by pulsing an annular plasma actuator.

Table 1: Flat plate experiments.

Case	U_∞ [cm/s]	Re_x
A	40	$4 \cdot 10^3$
B	100	$10 \cdot 10^3$
C	150	$15 \cdot 10^3$

exchanger; tunnel temperature was typically held constant at 60 °F. The inlet velocity is controlled by a valve upstream of the test section settling chamber which contains turbulence reducing screens and honeycomb. A boundary bleed slot was located approximately 20 cm downstream of the grid and a trip was located immediately downstream of the bleed slot. The plasma actuator insert was located approximately 110 cm downstream of the bleed. The tunnel speed used in the current experiments was in the range 0.4-3 m/s. Due to contamination of the lower wall boundary layer, the plasma actuators were mounted on a splitter plate. The actuator interface was located 15 cm from the leading edge of the splitter plate. Details of the baseline flow are presented in Jacob *et al.* (2004).

Velocity profiles for Case A are shown in Figure 7; u' and $u'v'$ are shown in Figure 8 and 9, respectively. Each profile curve is separated by $\Delta = 3.3$ mm. Note that the PFC actuator is located just upstream of the 3rd velocity profile station. Once the actuator is turned on, the upstream most profile is only slightly deviated from the baseline nearly Blasius profile (see Jacob *et al.*, 2004, for more discussion). The difference in the free-stream velocity between the unactuated and actuated states increases as we near the plasma region. This is indicative of flow being accelerated towards the plasma. Downstream of the plasma region, the velocity within the viscous region is increased and is no longer monotonic, and peaks around 0.25 cm, lower than seen in the quiescent case. The peak jet velocity increases and moves away from the wall as it moves downstream. Though not shown, if we examine v, we see that the magnitude is greatly increased immediately at the plasma region. This rapidly decays, but v is increased near the wall, reverses direction, then increases again. Values for all fluctuations are increased within the viscous layer; u' in particular has a peak located at the maximum value of u and generally follows the same trend (Figure 8). Values for v', while greater in the wall region, are lower in the free-stream, both upstream and downstream of the actuator. The

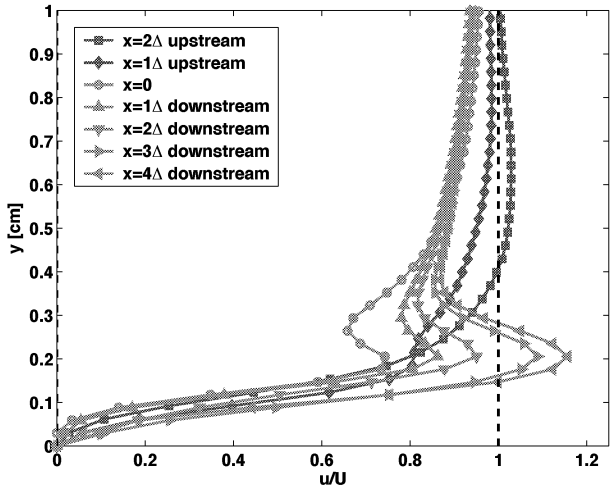

Figure 7: Case A; profiles of u/U.

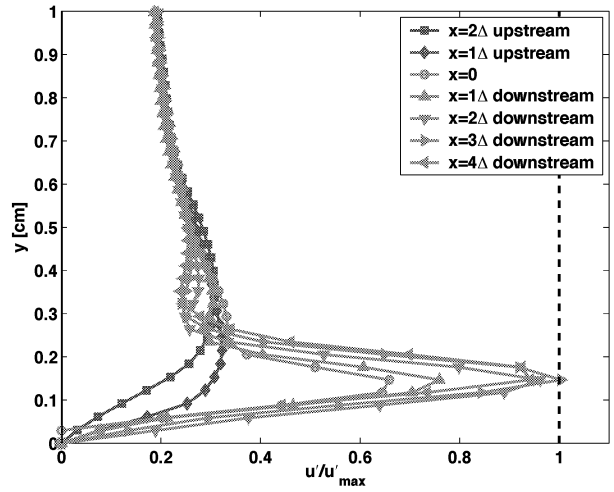

Figure 8: Case A; profiles of u'/u'_{max}.

Reynolds stress estimates peak within the viscous layer then decay in the free-stream to their non-controlled counterparts (Figure 9). Both u' and $u'v'$ are approximately 3 times larger than corresponding values seen in the baseline flow.

Figures 10 and 11 show similar profiles for u/U and u', respectively, for Case B. In this case, the free-stream velocity is now nearly the same as the plasma induced jet. Note that while the mean velocity is only slightly deviated from the baseline, and the maximum value is smaller than the baseline, the fluctuating values are still significant and nearly 3 times larger than those seen in the baseline flow. The same results, though not shown, are observed for Case C. Thus, at these free-stream velocities, the presence of the plasma induced jet itself does not appear to have a large impact on the flow field. The turbulent fluctuations, however, may have a significant effect.

Displacement thickness, δ^*, and momentum thickness, θ, are calculated for these cases using the equations below.

$$\delta^* = \int_0^h (1 - \frac{u}{u_e}) dy \tag{3}$$

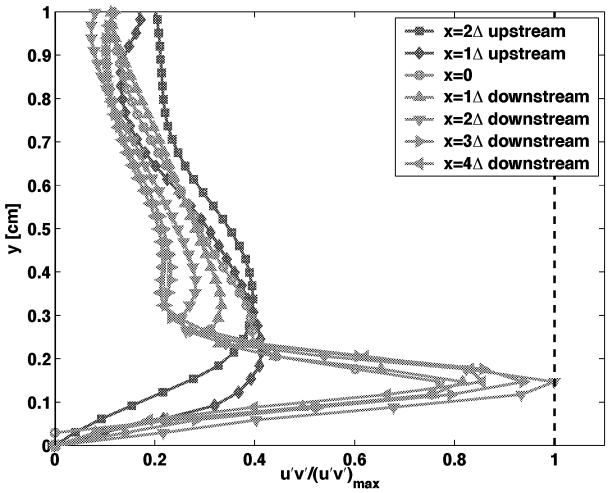

Figure 9: Case A; profiles of $u'v'/u'v'_{max}$.

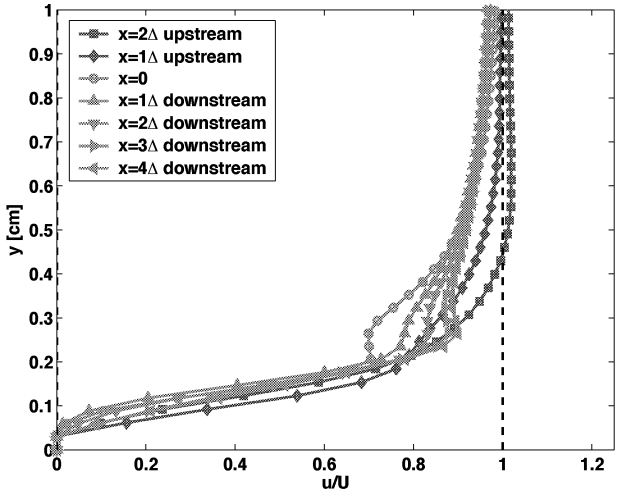

Figure 10: Case B; profiles of u/U.

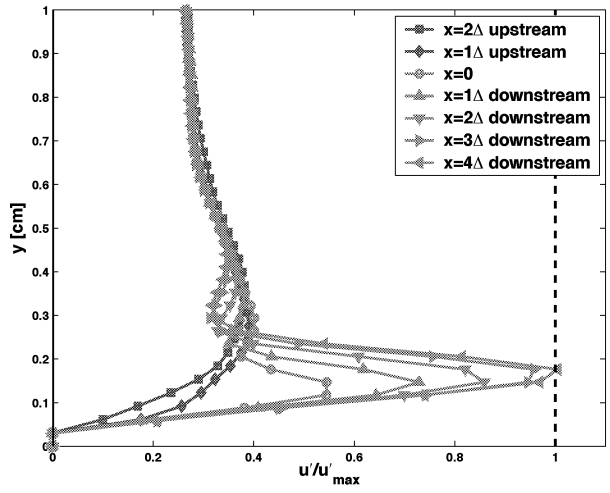

Figure 11: Case B; profiles of u'/u'_{max}.

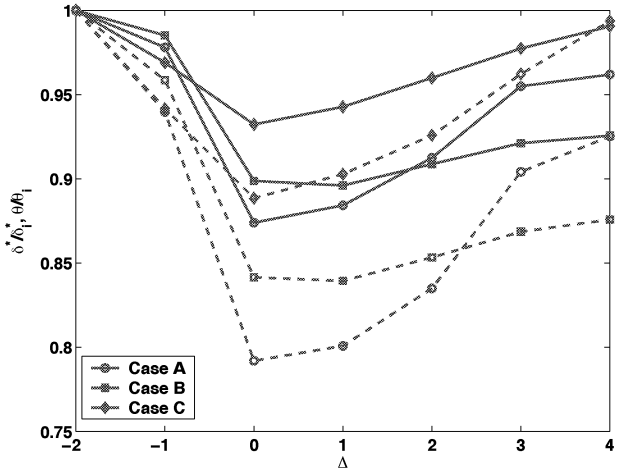

Figure 12: Displacement, δ^*, (solid line) and momentum, θ, (dashed line) thicknesses for the Case A, B, and C.

$$\theta = \int_0^h \frac{u}{u_e}(1 - \frac{u}{u_e})dy \tag{4}$$

Results are shown in Figure 12, normalized to the initial values determined from the first profile station for each Case. In each case, both δ^* and θ are reduced as the flow nears the plasma region, reaching a minimum at the interface. Downstream, both δ^* and θ increase to nearly their initial value as the jet is diffused. Note that in the lower speed cases, the reduction in δ^* and θ are larger, indicating that the plasma induced jet has a larger impact on the flow. Note that for Case C, δ^* and θ are reduced by 5% and 10%, respectively, compared to 13% and 20%, respectively, for Case A.

Separation Control on a Low Pressure Turbine Blade

Following the observations of the flat plate experiments, the PFC actuator has been applied to the control of separated flows in a 2D low pressure turbine blade cascade at low Re. The experiments were conducted in the UK Low-Speed Wind Tunnel, which is a low-turbulence, open-circuit, blow-down wind tunnel with a computer controlled, 7.5 hp motor driving a radial fan. Upstream of the nozzle, a vibration damper, flow straightener and turbulence damping screens condition the flow. The nozzle has a contraction ratio of 6.7, and the test section has a cross-section of 0.2 m×0.4 m. The nominal FSTI without the grid was measured with a hot-wire anemometer to be $\sim 0.6\%$. A set of identical P&W PAK-B turbine blade models with a chord length of 114 mm, a span of 203 mm and a suction surface length (SSL) of 152 mm are used in the experiments. The plasma actuator was mounted onto Kapton sheets and placed directly on the blade surface. The actuator interface is located at 65% of the SSL (0.65 SSL), where the

Table 2: LPT experiments, all at $Re = 3 \cdot 10^4$.

Case	Control	Duty Cycle	F_{pulse}
I	No	–	–
II	Yes	100%	–
III	Pulsed	50%	10 Hz

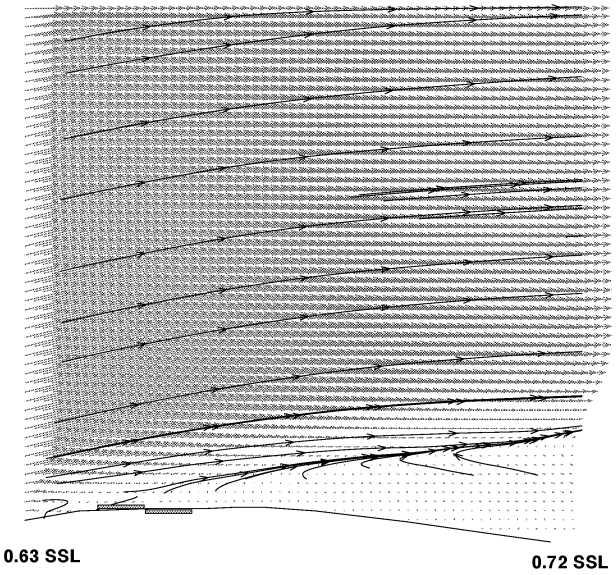

Figure 13: Separation region over LPT, Case I.

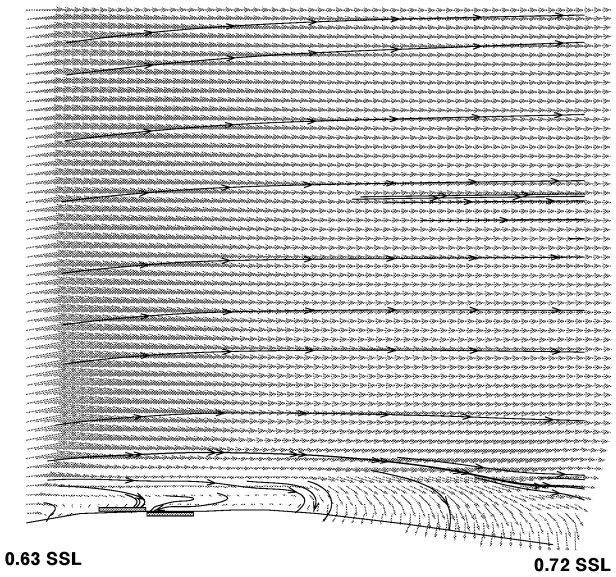

Figure 14: Separation region over LPT, Case II.

separation point has been previously shown to be located (e.g., McQuilling and Jacob, 2004). Note that at this point, $Re_x = 19.5 \cdot 10^4$, an order of magnitude larger than that seen in the flat plate experiments discussed above.

Figure 13 shows the velocity field over the blade without the PFC actuator turned on. Gross separation is clearly seen. The separation is steady, while the shear layer fluctuates in size and strength. Figures 14 and 15 show the corresponding velocity fields for Case II and III, respectively, where the PFC has been actuated. Note than in both cases, the flow is attached, and reversed flow is seen at the PFC interface where flow from the free-stream is being entrained by the plasma jet. While a "trapped" vortex is present in Figure 15 from the pulsed actuator, no other appreciable difference is present in the 100% and 50% duty cycles beyond some minor varia-

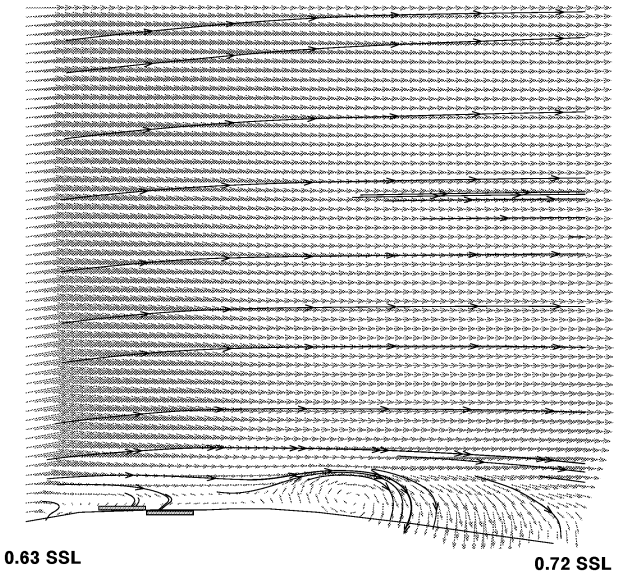

Figure 15: Separation region over LPT, Case III.

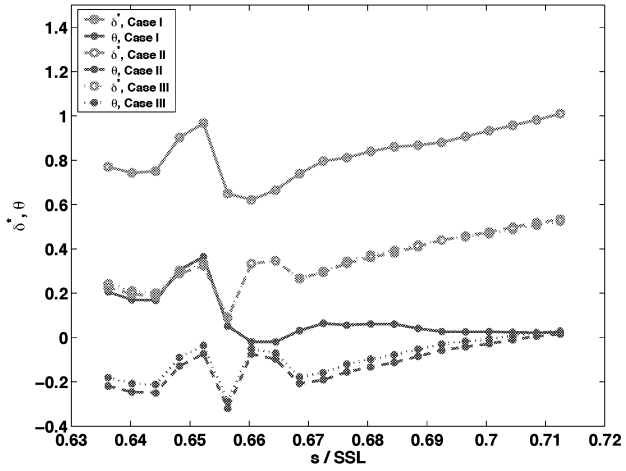

Figure 16: Displacement, δ^*, (solid line) and momentum, θ, (dashed line) thicknesses for the Case I, II, and III.

tions in the velocity fluctuation quantities. Displacement, δ^*, and momentum, θ, thicknesses are calculated using equations 3 and 4 and are shown in Figure 16. δ^* is nearly constant downstream of the actuator. While they are both reduced for the actuated cases, the 100% and 50% duty cycles are nearly identical.

SUMMARY

Measurements from the present work agree with many of the previous studies discussed above that show an increase in velocity in the region of the PFC actuator. Note that the increase in velocity, while significant, is well within the viscous region and requires detailed measurements very near the wall. The increase is also very short-lived and the flow reverts to a profile similar to the upstream flow not far downstream. Both displacement and momentum thicknesses are decreased due to the PFC actuator. As free-stream velocity is increased, the influence of the plasma region on the near-wall flow becomes less influential; thus, a corresponding increase in actuator power is also required. However, the increase in near-wall velocity fluctuations is significant and long-lived, even for cases where the mean velocity profile is not significantly affected, and has the ability to control flows even at moderately high speeds with low power input by acting as an active boundary layer trip.

REFERENCES

R. Rivir, A. White, C. Carter, B. Ganguly, A. Forelines, & J. Crafton. "Turbine Flow Control, Plasma Flows." *AIAA 41st Aerospace Sciences Meeting & Exhibit.* AIAA Paper 2003-6055, Reno, NV, Jan. 2003.

C. Suchomel, D. Van Wie, and D. Risha. "Perspectives on Cataloguing Plasma Technologies Applied to Aeronautical Sciences." *34th AIAA Plasmadynamics and Laser Conference.* AIAA Paper 2003-3852, Orlando, FL, June, 2003.

J. D. Jacob. "Time Resolved PIV Measurements of Plasma Based Flow Control." Air Force Summer Faculty Fellowship Program Final Report, AFRL/WPAFB, July, 2004.

T. E. McLaughlin, M. D. Munska, J. P. Vaeth, T. E. Dauwalter, J. R. Goode, and S. G. Siegal. "Plasma-Based Actuators for Cylinder Wake Vortex Control." *AIAA 2nd Flow Control Meeting*, AIAA Paper 2004-2129, Portland, OR, June, 2004.

T. C. Corke, C. He, and M. P. Patel. "Plasma Flaps and Slats: An Application of Weakly Ionized Plasma Actuators." *AIAA 2nd Flow Control Meeting*, AIAA Paper 2004-2127, Portland, OR, June, 2004.

M. Post and T. C. Corke. "Separation Control Using Plasma Actuators – Dynamic Stall Control on an Oscillating Airfoil." *AIAA 2nd Flow Control Meeting*, AIAA Paper 2004-2517, Portland, OR, June, 2004.

C. L. Enloe, T. E. McLaughlin, R. D. VanDyken, K. D. Kachner, E. J. Jumper, and T. C. Corke. "Mechanisms and Responses of a Single Dielectric Barrier Discharge Plasma Actuator: Plasma Morphology." *AIAA Journal*, **42**, No. 3, March, 2004, pp. 589–594.

C. L. Enloe, T. E. McLaughlin, R. D. VanDyken, K. D. Kachner, E. J. Jumper, T. C. Corke, M. Post, and O. Haddad. "Mechanisms and Responses of a Single Dielectric Barrier Discharge Plasma Actuator: Geometric Effects." *AIAA Journal*, **42**, No. 3, March, 2004, pp. 595–604.

S. Leonov, V. Bityurin, N. Savischenko, A. Yuriev, and V. Gromov. "Influence of Surface Electrical Discharge on Friction of Plate in Subsonic and Transonic Airfoil." *AIAA 39th Aerospace Sciences Meeting & Exhibit.* AIAA, 2001, Paper 2001-0640.

J. D. Jacob, R. Rivir, C. Carter, and J. Estevadeordal. "Boundary Layer Flow Control Using AC Discharge Plasma Actuators." *AIAA 2nd Flow Control Meeting*, AIAA Paper 2004-2128, Portland, OR, June, 2004.

M. J. Sholl and Ö. Savaş. "A Fast Lagrangian PIV Method for Study of General High-Gradient Flows." *AIAA 35th Aerospace Sciences Meetins & Exhibit.* Reno, NV, 1997. Paper 97-0493.

L. Tsuei and Ö Savaş. "Treatment of Interfaces in Particle Image Velocimetry." *Experiments in Fluids*, **29**, pp. 203–214, 2000.

M. McQuilling and J.D. Jacob, "Effect of Chord Location on Separation Control with Vortex Generator Jets on Low Pressure Turbine Blades." *AIAA 2nd Flow Control Conference*, Portland, OR, Paper 2004-2205.